Weak localization in a lateral superlattice with Rashba and Dresselhaus spin-orbit interaction

D. C. Marinescu
Department of Physics and Astronomy, Clemson University, Clemson, South Carolina 29634, USA

Andrei Manolescu
School of Science and Engineering, Reykjavik University, Menntavegur 1, IS-101 Reykjavik, Iceland
(Received 20 December 2011; revised manuscript received 24 February 2012; published 5 April 2012)

We calculate the weak localization (WL) correction to the conductivity of a lateral superlattice (LSL) with Rashba (R)-Dresselhaus (D) spin-orbit interaction (SOI). The superlattice is modeled as a sequence of parallel wires that support tunneling between adjacent sites, leading to the formation of extended Bloch states along its axis and a miniband in the energy spectrum. Our results, obtained by calculating the eigenvalues of the Cooperon operator in the diffusion approximation, indicate that the electron dephasing rate that determines the antilocalization correction is enhanced by a term proportional with the LSL potential and the bandwidth. Within the same formalism, the spin-relaxation rates associated with the localization corrections are found to exhibit a strong anisotropy dictated by the relative strength of the two SOI couplings, as well as by the orientation of the LSL axis.

DOI: 10.1103/PhysRevB.85.165302 PACS number(s): 73.20.Fz, 71.70.Ej, 73.21.Hb, 72.25.Rb

I. INTRODUCTION

A lateral superlattice (LSL), created when a periodic potential acts along a given direction in a two-dimensional (2D) system, can be most generally described as a sequence of parallel quasi-one-dimensional wires that appear from the confinement of the electrons in the potential wells. In particular, in systems with spin-orbit interaction (SOI) this setup offers the opportunity of investigating the interplay between geometric and spin-dependent effects. Experimentally, the realization of this situation was obtained early on in semiconductor structures,[1] but more recently was revealed to exist in other circumstances, such as the vicinal stepped surface of Au(111).[2] Theoretical investigations of these systems have revealed interesting features that stem from an energy spectrum that showcases chiral minibands spin split by the spin-orbit coupling,[3,4] such as a modulated spin polarization,[5–7] enhanced plasmonic excitation frequency along the LSL axis,[8] or a SOI-induced modulation effect on the electric conductivity predicted to exist even at high temperatures.[9] Measurements of the spin-relaxation times in these systems have indicated that the strong spatial anisotropy is determining specific behavior, leading to the possibility of controlling such system parameters through the growth process of the LSL.[10]

In this work we are inspired by the latter results to investigate the modulation effect induced by the Rashba (R) and Dresselhaus (D) SOI on the electric conductivity, as well as the anisotropy of the spin-relaxation rates within a unitary formalism derived in the weak localization approximation. Considering that the physical properties of the LSL are tuned in the growth process, our analysis bridges the theoretical discussion of isolated quantum wires[11,12] with that of the isotropic 2D systems.[13,14] In the following considerations, this continuous transition between the two limiting cases is parametrized by the miniband width that is allowed to develop in the single-particle energy spectrum as a result of tunneling between adjacent wires, when the single-particle states in the wells are extended into Bloch waves along the direction of the SL axis.

At the center of this investigation is the well known result that identifies the quantum interference of the electron trajectories that results from multiple scattering events as the source of the decrease in conductivity. The coupling between time-reversed trajectories, described by the convolution in phase space of an advanced and retarded Green's functions, defines the Cooperon or propagator operator. When averaged over the impurity distribution, the Cooperon presents integrable divergencies in the momentum space that determine the corrections to the conductivity in the weak localization approximation.[15] In the case of SOI systems the poles of the Cooperon involve the spin-relaxation rates along the three spatial directions. This results from the nonconservation of the electron spin in systems with SOI, when the spin components S_i $(i = x,y,z)$ undergo a relaxation process with time τ_{S_i}, proportional with the SOI strength, that introduces an additional channel of coherence loss in the the interference of the time-reversed trajectories.[13,14,16] The positive correction to the conductivity, the antilocalization term, is independent of SOI and results from the interference of states with opposite momenta and opposite spin that are odd under time-reversal symmetry.

The extension of this formalism to an LSL with Rashba-Dresselhaus SOI indicates that the scattered Bloch states are responsible for generating interference terms that remain different from zero in the localization limit, a result that appears independent of the strength of SOI or its origin. This is a consequence of the additional localization imposed by the external potential along the LSL axis leading to an enhancement of the dephasing rate that increases the antilocalization correction. At the same time, the spin-relaxation rates reflect the interference of the two spin-orbit couplings, as well as the anisotropy of the system embodied by the different diffusion coefficients. This generates possibilities of experimental control of the spin-relaxation process that can be considerably reduced for propagation along certain spatial directions, as was experimentally observed recently in Ref. 10.

Our paper starts by introducing a general description of the system in Sec. II, followed by an outline of the computation

algorithm presented in Sec. III. A discussion of the results is presented in Sec. IV.

II. THEORETICAL MODEL

We consider a 2D electron system with spin-orbit interaction that originates in the asymmetry of the quantum well (Rashba) as well as in the inversion asymmetry of the crystal (Dresselhaus), both linear in the particle momentum. While the strength of the Dresselhaus interaction β is determined by the atom structure of the material, the α that describes the Rashba coupling is known to be sensitive to externally applied electric fields, allowing for great liberty in choosing its magnitude. The corresponding single-particle Hamiltonian is customarily written in the natural coordinate system imposed by the two interactions along the crystallographic directions [110],[1$\bar{1}$0] renamed here $\{\hat{x}',\hat{y}'\}$, when in terms of the electron momentum $\mathbf{p} = \{p_{x'}, p_{y'}\}$ and spin $\sigma = \{\sigma_{x'},\sigma_{y'},\sigma_{z'}\}$

$$H'_{\rm SO} = \alpha(\sigma_{x'} p_{y'} - \sigma_{y'} p_{x'}) + \beta(\sigma_{x'} p_{x'} - \sigma_{y'} p_{y'}). \quad (1)$$

The external periodic potential, described as a sequence of infinitely attractive quantum wells separated by a distance a, is considered to act along a direction $\hat{x}$ rotated in respect with $\hat{x}'$ by an angle φ,

$$V(x) = -V_0 \sum_l \delta(x - la). \quad (2)$$

In this approximation, in each well, a single bound state of energy $\epsilon_0 = -\frac{\hbar^2\kappa^2}{2m^*}$ associated with an eigenstate $\nu(x) = \sqrt{\kappa} e^{-\kappa|x|}$, with $\kappa = m^* V_0/\hbar^2$ (m^* is the effective electron mass). Allowing for weak tunneling between the quasi-one-dimensional wires thus constructed, the single-particle state inside the wells broadens into a miniband whose width, estimated within the tight-binding approximation, is $\Delta = 2\epsilon_0 e^{-2\kappa a}$.

Since the SL axis introduces a preferential direction in the 2D plane, different from the axes defined by the SOI couplings, it is necessary to rewrite the Hamiltonian $H'_{\rm SO}$ in the new system of axis $\{\hat{x},\hat{y}\}$. The rotation of angle φ leaves the Rashba term in Eq. (1) unchanged, but modifies the Dresselhaus contribution. The new Hamiltonian, which includes the kinetic term as well as the external potential, is therefore

$$H = \frac{p^2}{2m^*} + V(x) + (\alpha - \beta \sin 2\varphi) p_y \sigma_x - (\alpha + \beta \sin 2\varphi) p_x \sigma_y. \quad (3)$$

The exact solution of the eigenvalue-eigenfunction problem of the Hamiltonian given in Eq. (3) has been extensively studied by both analytical[7] and numerical methods.[4] These results indicate the existence of chiral split minibands whose width is determined by the interference between the broadening effect of the single-particle states in the presence of interwell tunneling and spin-orbit coupling that involves the periodic momentum along the LSL axis. In the weak localization problem, the dominant energy scale is introduced by the uncorrelated scattering on impurities, $\hbar/\tau_0$. The scattering is assumed to be isotropic and elastic such that the relaxation time τ_0 is related to the strength of the impurity potential u^2 for a single spin density of states at the Fermi surface N_0 through $\tau_0^{-1} = 2\pi N_0/\hbar u^2$. In this regime, when $\hbar/\tau_0$ is much larger than either the miniband width or the SOI coupling, the effect of the spin-orbit interaction is treated perturbatively in an approximation that allows its reduction to a separate scattering mechanism by means of a non-Abelian unitary transformation in the spin space.[17,18] The spin-dependent generator of the transformation $\mathbf{A} = \{A_x, A_y\}$ is obtained by exploiting the linear coupling of the electron momentum to the spin in the SOI terms such that

$$\mathbf{A}(\sigma) = m^*\{[\beta \cos 2\varphi\, \sigma_x - (\alpha + \beta \sin 2\varphi)\sigma_y]\hat{e}_x + [(\alpha - \beta \sin 2\varphi)\sigma_x - \beta \cos 2\varphi \sigma_y]\hat{e}_y\}/\hbar. \quad (4)$$

Thus, in a first order approximation in the spin-orbit terms, H can be obtained from a single-particle Hamiltonian in the absence of SOI through

$$H = e^{-i\mathbf{A}\cdot\mathbf{r}} H_0 e^{i\mathbf{A}\cdot\mathbf{r}}, \quad (5)$$

where

$$H_0 = \frac{p^2}{2m^*} + V(x). \quad (6)$$

The equivalence between Eqs. (3) and (5) is proven by expanding the unitary operator, which commutes with the periodic potential, in first order in the SOI coupling constants and by neglecting the second-order terms, considered to be much smaller than the energy scale set by impurity scattering.

An eigenstate of H_0 is built as a Bloch function from the single-particle states inside the wire $\nu(x)$, multiplying an up or down spin state $\chi_\sigma = \{|\uparrow\rangle, |\downarrow\rangle\}$,

$$\psi_{k_x,k_y,\sigma} = \frac{1}{\sqrt{L_y}} e^{ik_y y + ik_x x} \xi_{k_x}(x)\chi_\sigma, \quad (7)$$

with

$$\xi_{k_x}(x) = \frac{1}{\sqrt{N}} \sum_l e^{-ik_x(x-la)} \nu(x - la). \quad (8)$$

k_x is subject to periodic boundary conditions and is given by $k_x = \frac{2\pi}{Na} j$, where $j \in [-N/2, N/2]$. The single-particle energy is written, with respect to the minimum of the band, as

$$\epsilon_{\mathbf{k}\sigma} = \frac{\hbar^2 k_y^2}{2m^*} + \frac{\Delta}{2}(1 - \cos k_x a). \quad (9)$$

This spectrum describes an isolated quantum wire in the limit $e^{-\kappa a} \sim 0$ when $\Delta \sim 0$, while the isotropic 2D case is reached when $k_x a \ll 1$ and the effective electron mass constrains the relationship between Δ and a through $(m^*)^{-1} = \Delta a^2/2\hbar^2$.

The eigenstates of the Hamiltonian H_0 are employed in obtaining the advanced and retarded spin-independent Green's functions $G^{\pm}(\omega,\mathbf{k}) = (\hbar\omega - \epsilon_{\mathbf{k}} \pm \frac{i\hbar}{2\tau_0})^{-1}$.

In the presence of SOI, these Green's functions are modified by the unitary transformation generated by $\mathbf{A}(\sigma)$ in Eq. (4), such that in real space, for particle coordinates $\mathbf{r}$ and $\mathbf{r}'$, it is obtained:

$$\mathcal{G}^{\pm}_{\sigma}(\mathbf{r},\mathbf{r}') = e^{i\mathbf{A}(\sigma)\cdot(\mathbf{r}-\mathbf{r}')} G^{\pm}(\mathbf{r},\mathbf{r}'). \quad (10)$$

Expanding Eq. (10) up to second order in $\mathbf{A}(\sigma)$, we obtain

$$\mathcal{G}^{\pm}_{\sigma}(\mathbf{r},\mathbf{r}') = [1 - i\mathbf{A}\cdot\Delta\mathbf{r} - (\mathbf{A}\cdot\Delta\mathbf{r})^2/2] G^{\pm}(\mathbf{r},\mathbf{r}'), \quad (11)$$

where $\Delta\mathbf{r} = \mathbf{r} - \mathbf{r}'$.

The theory of the localization corrections to the conductivity is built around the the propagator operator or Cooperon which represents the convolution in phase space of the retarded and the advanced functions Green's functions that correspond to the time-reversed trajectories of two different electrons indexed by their spin operators σ and ρ at the Fermi surface

$$\mathcal{P}^0(\mathbf{q},\Omega) = \int d(\hbar\omega) \sum_{\mathbf{p}} \mathcal{G}_\sigma^-(-\mathbf{p}+\mathbf{q},\omega+\Omega)\mathcal{G}_\rho^+(\mathbf{p},\omega). \tag{12}$$

The matrix representation of the propagator occurs in the $S_1 \bigotimes S_2$, where S_1 and S_2 are the two-dimensional spin spaces associated with each spin 1/2, denoted as σ and ρ. From Eq. (11) we write, with $\tilde{\mathbf{A}} = \mathbf{A}(\sigma) + \mathbf{A}(\rho)$,

$$\mathcal{P}^0 = e^{i\tilde{\mathbf{A}}\cdot\mathbf{r}} P^0, \tag{13}$$

where

$$\begin{aligned} P^0(\mathbf{q},\Omega) &= \int d(\omega) \sum_{\mathbf{p}} G^-(-\mathbf{p}+\mathbf{q},\omega+\Omega)G^+(\mathbf{p},\omega) \\ &= \frac{2\pi N_0 \tau_0}{\hbar}\left[1 + i\Omega\tau_0 - \left(D_x q_x^2 + D_y q_y^2\right)\tau_0\right]. \end{aligned} \tag{14}$$

This result, obtained from the expansion of the two Green's functions in second order in $\tau_0/\hbar$, introduces the diffusion coefficients along the two axes D_x and D_y which are defined in terms of the single spin density of states at the Fermi surface N_0. Assuming full miniband occupancy, that is, $k_x \in [-\pi/a,\pi/a]$, N_0 is calculated as

$$\begin{aligned} N_0 &= \sum_{\mathbf{k}} \delta(\epsilon_{\mathbf{k}} - \epsilon_F) \\ &= \frac{m^*}{\pi^2\hbar^2(ak_{Fy})} \int_0^\pi \frac{d(k_x a)}{\sqrt{1 - \frac{\Delta}{2\epsilon_F}(1-\cos k_x a)}} \\ &= \frac{m^*}{\pi^2\hbar^2(ak_{Fy})} \mathcal{E}\left(\sqrt{\frac{\Delta}{\epsilon_F}}\right), \end{aligned} \tag{15}$$

where $k_{Fy} = \sqrt{2m^*\epsilon_F/\hbar^2}$ is the maximum value of the $\hat{y}$ momentum and $\mathcal{E}(x)$ is the complete elliptical function of the second kind.[19] In Eq. (15) the summation over states was transformed into an integral by using the periodic boundary conditions and the evenness of the interval of integration in k_x and k_y.

The Fermi energy ϵ_F is correlated with the particle density n through

$$\begin{aligned} n &= \sum_{\mathbf{k},\sigma} \theta(\epsilon_F - \epsilon_{\mathbf{k}}) \\ &= \frac{2}{\pi^2 a} \int_0^\pi d(k_x a) \sqrt{\frac{2m^*}{\hbar^2}\left[\epsilon_F - \frac{\Delta}{2}(1-\cos k_x a)\right]} \\ &= \frac{4k_{Fy}}{\pi a} \mathcal{K}\left(\sqrt{\frac{\Delta}{\epsilon_F}}\right), \end{aligned} \tag{16}$$

with $\theta(\epsilon_{\mathbf{k}} - \epsilon_F)$ the Heaviside function and $\mathcal{K}(x)$ the complete elliptic integral of the first kind.[19]

The diffusion coefficients $D_{x,y}$ in Eq. (14) are

$$D_{x,y} = \frac{\tau_0}{N_0} \sum_{\mathbf{k}} \left(\frac{1}{\hbar}\frac{\partial\epsilon_{k_x,k_y}}{\partial k_{x,y}}\right)^2 \delta(\epsilon_{\mathbf{k}} - \epsilon_F). \tag{17}$$

By performing the summation over $\mathbf{k}$, we obtain

$$\begin{aligned} D_y &= \left(\frac{\hbar k_{Fy}}{m^*}\right)^2 \tau_0 \frac{\mathcal{K}\left(\sqrt{\frac{\Delta}{\epsilon_F}}\right)}{\mathcal{E}\left(\sqrt{\frac{\Delta}{\epsilon_F}}\right)}, \\ D_x &= \frac{\tau_0}{\mathcal{E}\left(\sqrt{\frac{\Delta}{\epsilon_F}}\right)} \left(\frac{\Delta a}{2\hbar}\right)^2 \int_0^\pi d(k_x a) \\ &\quad \times \frac{\sin^2 k_x a}{\sqrt{1 - \frac{\Delta}{2\epsilon_F}(1-\cos k_x a)}} \\ &= \frac{\tau_0}{\mathcal{E}\left(\sqrt{\frac{\Delta}{\epsilon_F}}\right)} \left(\frac{\Delta a}{2\hbar}\right)^2 B\left(\frac{3}{2},\frac{3}{2}\right) F\left(\frac{3}{2},\frac{1}{2},3;\frac{\Delta}{\epsilon_F}\right), \end{aligned} \tag{18}$$

where $B(x,y)$ is the β function, while $F(\alpha,\beta,\gamma;x)$ is the Gauss hypergeometric series.[19]

These results are illustrated in Fig. 1 in the case of a GaAs LSL with an electron concentration of $n = 2 \times 10^{11}$ cm^{-2}. The variable parameter of the problem is Δ, the miniband width that can be set by adjusting the periodic potential. The Fermi energy, plotted in the inset, is determined self-consistently by imposing that for every Δ value, assuming a full occupation of the miniband, that is, $k_x \in [-\pi/a,\pi/a]$, the total number of particles is given by Eq. (16).

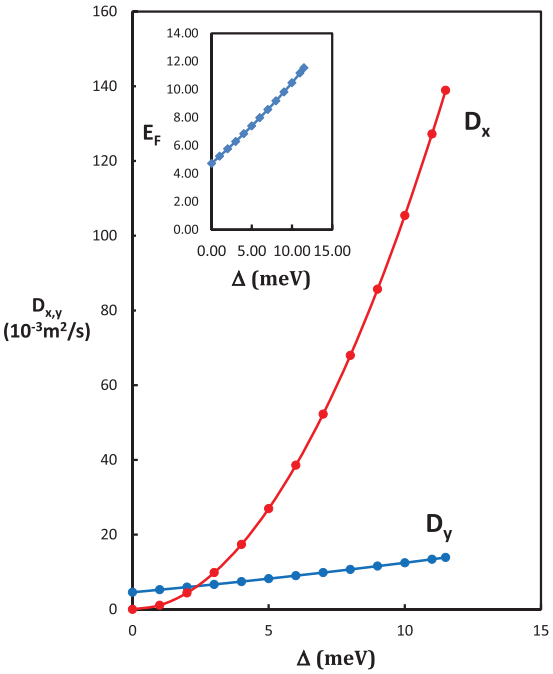

FIG. 1. (Color online) The anisotropy of the diffusion coefficients as a function of the miniband width Δ (expressed in meV) in a GaAs lateral superlattice with $a = 30$ nm and $n = 2 \times 10^{11}$ cm^{-2}. In the inset, the variation of the Fermi energy E_F is illustrated as a function of the miniband width Δ (both expressed in meV) in a GaAs lateral superlattice with $a = 30$ nm and $n = 2 \times 10^{11}$ cm^{-2}.

III. THE COOPERON EIGENVALUES

The logarithmic corrections to the conductivity are given by the eigenvalues of the impurity-configuration averaged propagator $\mathcal{P}$ calculated in the limit of $\mathbf{q}\to 0$. $\mathcal{P}$ satisfies the following Dyson equation:

$$\mathcal{P}=u^2+u^2\mathcal{P}^0(\mathbf{q},\Omega)\mathcal{P}(\mathbf{q},\Omega). \tag{19}$$

A solution to Eq. (19) is easily obtained within the Hilbert space of $\mathcal{P}^0$, where for an eigenfunction ψ_{jm}, indexed by the quantum numbers of a system of two spins jm, an eigenvalue Λ_{jm} satisfies

$$\int d^2r'\mathcal{P}^0(\mathbf{r},\mathbf{r}')\Psi_{jm}(\mathbf{r}')=\Lambda_{jm}\Psi_{jm}(\mathbf{r}). \tag{20}$$

In this representation, $\mathcal{P}^0(\mathbf{q},\Omega)=\sum_{jm}\Lambda_{jm}\Psi_{jm}(\mathbf{r})\Psi_{jm}(\mathbf{r}')$ and consequently, from Eq. (19),

$$\mathcal{P}=\sum_{jm}\frac{u^2}{1-u^2\Lambda_{jm}}\Psi_{jm}(\mathbf{r})\Psi_{jm}(\mathbf{r}'). \tag{21}$$

Finally, the corrections to the conductivity for the x,y directions, respectively, are estimated as[14]

$$\Delta\sigma_{x,y}=-\frac{e^2D_{x,y}}{4\pi^2\hbar}\sum_{jm}\int\frac{d^2q}{(2\pi)^2}\frac{u^2}{1-u^2\Lambda_{jm}}. \tag{22}$$

Equation (20) is linearized in a standard procedure that involves the expansion of both $\mathcal{P}^0(\mathbf{r},\mathbf{r}')$ and $\Psi_{ij}(\mathbf{r}')$ up to second order in $\Delta\mathbf{r}$ that facilitates the expression of the spatial integral in terms of the derivatives of the Fourier transform of the propagator Eq. (14):[15]

$$\left[P^0|_{\mathbf{q}=0}+\frac{1}{2}\frac{\partial^2P^0}{\partial x^2}\bigg|_{\mathbf{q}=0}\left(\frac{\nabla_x}{i}+\tilde{A}_x\right)^2+\frac{1}{2}\frac{\partial^2P^0}{\partial y^2}\bigg|_{\mathbf{q}=0}\left(\frac{\nabla_y}{i}+\tilde{A}_y\right)^2\right]\Psi_{jm}(\mathbf{r})=\Lambda_{jm}\Psi_{jm}(\mathbf{r}). \tag{23}$$

A solution for the Cooperon eigenstate $\psi_{jm}(\mathbf{r})$ is proportional with the product in real space of two electron wave functions, associated, respectively, with the momentum $-\mathbf{k}+\mathbf{q}$ and $\mathbf{k}$ multiplied by a spin part χ_{jm} that can be expanded in the basis of the angular momentum eigenstates $|j,m\rangle$ that correspond to the sum of two 1/2 spins, $\{|0,0\rangle,|1,1\rangle,|1,0\rangle,|1,-1\rangle\}$. Thus,

$$\Psi_{jm}(\mathbf{r})=\tilde{\psi}(\mathbf{r})\chi_{jm}, \tag{24}$$

where the spatial part of the function is written, from Eq. (7), as

$$\tilde{\Psi}=e^{iq_xx+iq_yy}\tilde{\xi}(x). \tag{25}$$

$\tilde{\xi}(x)$ results from the overlap of periodic parts of the Bloch function [Eq. (8)]

$$\begin{aligned}\tilde{\xi}(x)&=\frac{1}{\sqrt{N}}\xi_{-k_x+q_x}(x)\xi_{k_x}(x)\\&=\frac{1}{\sqrt{N}}\sum_{l_1,l_2}e^{-i(-k_x+q_x)(x-l_1a)-ik_x(x-l_2a)}\\&\quad\times\nu(x-l_1a)\nu(x-l_2a)\\&=\sum_{l_1}e^{-iq_x(x-l_1a)}\nu^2(x-l_1a).\end{aligned} \tag{26}$$

In particular, the last equality recognizes that on account of the sharp decay of the single-well states $\nu(z)$, the Cooperon eigenfunction retains only the product of two functions ν that belong to the same well. The function $\tilde{\xi}(x)$ has the periodicity of the LSL, which allows its expansion in a Fourier series,

$$\tilde{\xi}(x)=\sum_G e^{i\frac{2\pi}{a}Gx}\tilde{\xi}_G, \tag{27}$$

with coefficients $\tilde{\xi}_G$ given by

$$\tilde{\xi}_G=\frac{1}{a}\int_{-a/2}^{a/2}dxe^{-i\frac{2\pi}{a}Gx}\tilde{\xi}(x)=\frac{4\kappa^2}{a\left[4\kappa^2+\left(q_x+\frac{2\pi}{a}G\right)^2\right]}. \tag{28}$$

With these choices for the spatial part, the equation satisfied by the spin eigenstate of the Cooperon is written, from Eq. (23),

$$\begin{aligned}u^{-2}\Bigg\{&1+i\Omega\tau_0-D_y\tau_0(q_y+\tilde{A}_y)^2-D_x\tau_0\Bigg[(q_x+\tilde{A}_x)^2\\&+2(q_x+\tilde{A}_x)\int_C dx\tilde{\xi}(x)\left(\frac{\nabla_x}{i}\right)\tilde{\xi}(x)\Bigg]\\&+\int_C dx\tilde{\xi}(x)\left(\frac{\nabla_x}{i}\right)^2\tilde{\xi}(x)\Bigg\}\chi_{jm}=\Lambda_{jm}\chi_{jm},\end{aligned} \tag{29}$$

where the integration is performed on the unit cell. From symmetry considerations,[20] $\int_C dx\tilde{\xi}(x)\nabla_x\tilde{\xi}(x)=0$, while

$$\mu=-\int_C dx\tilde{\xi}(x)\nabla_x^2\tilde{\xi}(x)\neq 0. \tag{30}$$

After a straightforward calculation using the simple model adopted here for the LSL, we find that

$$\begin{aligned}\mu=&\left\{\frac{2a\left(q_x^2+(2\kappa)^2\right)\sinh 2\kappa a}{(4\kappa)^3(\cosh 2\kappa a-\cos q_xa)}+\frac{a^2}{(4\kappa)^2(\cosh 2\kappa a-\cos q_xa)^2}\left[\left(q_x^2-(2\kappa)^2\right)(\cos q_xa\cosh 2\kappa a-1)-4\kappa q_x\sinh 2\kappa a\sin q_xa\right]\right\}\\&\times\left\{\frac{2a\sinh 2\kappa a}{(4\kappa)^3(\cosh 2\kappa a-\cos q_xa)}+\frac{a^2}{(4\kappa)^2(\cosh 2\kappa a-\cos q_xa)^2}(\cos q_xa\cosh 2\kappa a-1)\right\}^{-1}.\end{aligned} \tag{31}$$

In the weak tunneling regime, when $e^{-\kappa a}\ll 1$, Eq. (31) generates $\mu=4\kappa^2$, a finite contribution to the Cooperon equation that results from the interference of the periodic part of the Bloch waves. The opposite limit $\kappa a\ll 1$ describes the transition to the

2D regime, when $\mu = 0$. With this input, Eq. (29) becomes

$$[1 + i\Omega\tau_0 - D_y\tau_0(q_y + \tilde{A}_y)^2 - D_x\tau_0(q_x + \tilde{A}_x)^2 - D_x\tau_0\mu]\chi_{jm} = \Lambda_{jm}\chi_{jm}, \tag{32}$$

We introduce the total spin operator $\mathbf{J} = \hbar(\sigma + \rho)/2$, its projection J_z on the $\hat{z}$ axis, and the ladder operators $J^{\pm} = J_x \pm iJ_y = \hbar(\sigma_x \pm \sigma_y)/4$. In terms of these operators, when Eq. (4) is considered, Eq. (32) becomes

$$\begin{aligned} u^{-2}\big(&1 + i\Omega\tau_0 - \tau_0 D_x\mu - \tau_0 D_x\big\{q_x^2 + 2iq_x[(\bar{\alpha} - i\bar{\beta}e^{2i\varphi})J^+ - (\bar{\alpha} + i\bar{\beta}e^{-2i\varphi})J^-] \\ &+ 2(\bar{\alpha}^2 + \bar{\beta}^2 + 2\bar{\alpha}\bar{\beta}\sin 2\varphi)\big(J^2 - J_z^2\big) - (\bar{\alpha} - i\bar{\beta}e^{2i\varphi})^2(J^+)^2 - (\bar{\alpha} + i\bar{\beta}e^{-2i\varphi})^2(J^-)^2\big\} \\ &- \tau_0 D_y\big\{q_y^2 + 2q_y[(\bar{\alpha} + i\bar{\beta}e^{2i\varphi})J^+ + (\bar{\alpha} - i\bar{\beta}e^{-2i\varphi})J^-] \\ &+ 2(\bar{\alpha}^2 + \bar{\beta}^2 - 2\bar{\alpha}\bar{\beta}\sin 2\varphi)\big(J^2 - J_z^2\big) + (\bar{\alpha} + i\bar{\beta}e^{2i\varphi})^2(J^+)^2 + (\bar{\alpha} - i\bar{\beta}e^{-2i\varphi})^2(J^-)^2\big\}\big)|\chi_{jm}\rangle = \Lambda_{jm}|\chi_{jm}\rangle. \end{aligned} \tag{33}$$

An immediate solution to Eq. (33) is the singlet state $|0,0\rangle$ which corresponds to the antisymmetric, antiparallel orientation of the two electron spins. The other three modes are coupled for finite $\mathbf{q}$ and an analytical solution can be obtained only in certain cases, such as when $\bar{\alpha} = \bar{\beta}$.[14] In the limit of $\mathbf{q} \to 0$, however, the Cooperon eigenvalues can be calculated exactly, their meaning being associated with the effective scattering rate of the three components of the spin.

A. The dephasing rate and the antilocalization correction

The antilocalization (AL) correction to the conductivity is generated by the $|0,0\rangle$ eigenstate of the Cooperon which is odd under time reversal. From Eq. (33) the associated eigenvalue is

$$\Lambda_{00} = 1 + i\Omega\tau_0 - \tau_0 D_x\mu - \tau_0 D_x q_x^2 - \tau_0 D_y\tau_0. \tag{34}$$

The corresponding contribution to the conductivity is positive and is written from Eq. (22) as

$$\Delta(\sigma_{x,y})_{\mathrm{AL}} = \frac{e^2}{4\pi^2\hbar} D_{x,y} \sum_{\mathbf{q}} \frac{1}{D_x q_x^2 + D_y q_y^2 + \tilde{\tau}_\phi^{-1}}, \tag{35}$$

where $\tilde{\tau}_\phi^{-1} = -i\Omega + \tau_0 D_x\mu$. In the 2D limit, when $\mu = 0$, $\tau_\phi^{-1} = -i\Omega$ represents the inelastic dephasing time of the electrons that describes the loss of coherence between the time-reversed paths of the electrons. In contrast with the isotropic 2D case, the LSL value $\tilde{\tau}_\phi$ includes an additional contribution provided by the existence of the periodic potential and the associated Bloch function that generates second-order nonzero spatial derivatives of the eigenstate even in the limit of zero momentum. Physically, the enhancement of the dephasing rate is associated with the interference effect mediated by the Bloch function, which forces the time-reversed trajectories of the Cooperon particles to overlap less than in the isotropic case.

The summation over $\mathbf{q}$ in Eq. (35) needs to consider the fact that in the case of the LSL, the momentum q_x is defined only up to a reciprocal lattice vector. It is customary to redefine q_x inside the first Brillouin zone, such that the addition of multiples of the reciprocal lattice vectors becomes apparent, $q_x \to q_x + 2\pi l/a$, where l counts the number of wires N in the system. Therefore, the sum in $\mathbf{q}$ space is calculated as

$$\sum_{\mathbf{q}} = \frac{1}{(2\pi)^2}\int_{-\infty}^{\infty} dq_y \int_{-\pi/a}^{\pi/a} dq_x \sum_{l=-N/2}^{N/2}. \tag{36}$$

The discrete sum over N is estimated for large N and for $D_x \neq 0$ as

$$\begin{aligned} &\sum_{l=-N/2}^{N/2} \frac{1}{D_x\big(q_x + 2\pi l/a\big)^2 + D_y q_y^2 + \tilde{\tau}_\phi^{-1}} \\ &= \frac{a}{\sqrt{D_x\big(D_y q_y^2 + \tilde{\tau}_\phi^{-1}\big)}} \\ &\quad\times \frac{\sinh a\sqrt{\big(D_y q_y^2 + \tilde{\tau}_\phi^{-1}\big)/D_x^2}}{\cosh a\sqrt{\big(D_y q_y^2 + \tilde{\tau}_\phi^{-1}\big)/D_x^2} - \cos q_x a}. \end{aligned} \tag{37}$$

This expression considers contributions to the antilocalization corrections for all Brillouin zone, in contrast with the approximation used in Ref. 21 where only the $l = 0$ (first Brillouin zone) was counted. When $D_x = 0$, the summation over l reproduces simply the number of wires N.

The AL conductivity correction for the $\hat{x}$ and $\hat{y}$ axis, respectively, is obtained, with input from Eqs. (22) and (37) as

$$\begin{aligned} (\Delta\sigma_{x,y})_{\mathrm{AL}} &= \frac{e^2}{2\pi^2\hbar} D_{x,y} \int_0^{q_y^{\max}} \frac{dq_y}{2\pi} \int_{-\pi/a}^{\pi/a} \frac{dq_x}{2\pi} \frac{a}{\sqrt{D_x\big(D_y q_y^2 + \tilde{\tau}_\phi^{-1}\big)}} \frac{\sinh a\sqrt{\big(D_y q_y^2 + \tilde{\tau}_\phi\big)/D_x^2}}{\cosh a\sqrt{\big(D_y q_y^2 + \tilde{\tau}_\phi^{-1}\big)/D_x^2} - \cos q_x a} \\ &= \frac{e^2}{2\pi^2\hbar} D_{x,y} \int_0^{q_y^{\max}} \frac{dq_y}{2\pi} \frac{1}{\sqrt{D_x\big(D_y q_y^2 + \tilde{\tau}_\phi^{-1}\big)}} \\ &= \frac{e^2}{2\pi^2\hbar} \frac{D_{x,y}}{\sqrt{D_x D_y}} \ln\left(\frac{\sqrt{D_y} q_y^{\max} + \sqrt{D_y\big(q_y^{\max}\big)^2 + \tilde{\tau}_\phi^{-1}}}{\sqrt{\tilde{\tau}_\phi^{-1}}}\right) \simeq \frac{e^2}{4\pi^2\hbar} \frac{D_{x,y}}{\sqrt{D_x D_y}} \ln\left(\frac{\tau_\phi}{\tau_0}\right), \end{aligned} \tag{38}$$

where we introduced the usual cutoff for $q_y^{\max} = \sqrt{\tau_0^{-1}/D_y}$. In the case of an isotropic system $D_x = D_y$ and we recover the usual expression of the AL correction, while for an isolated wire, when $D_x = 0$, the corresponding correction to the conductivity is obtained as

$$(\Delta\sigma_y)_{\rm AL} = \frac{e^2}{2\pi\hbar}\frac{1}{a}\int_{-\infty}^{\infty}\frac{dq_y}{D_y q_y^2 + \tilde{\tau}_\phi^{-1}} = \frac{e^2}{2\pi\hbar}\frac{1}{a}\frac{\sqrt{D_y}}{\tilde{\tau}_\phi^{-1}} = \frac{e^2}{2\pi\hbar}\frac{l_\phi}{a}, \tag{39}$$

with $l_\phi = \sqrt{D_y}/\tilde{\tau}_{\phi^{-1}}$ the dephasing length along the $\hat{y}$ direction.[21] The limit of the 2D system is obtained by constraining the effective band mass $(\Delta a^2/2\hbar)^{-1}$ to reach the effective mass value along the $\hat{y}$ direction m^*.

B. Spin-relaxation rates and the localization correction

The spin-relaxation rates involved in the localization corrections to the conductivity are obtained from the other three solutions to the Cooperon eigenvalue equation (33) estimated in the limit $\mathbf{q} \to 0$. The localization correction corresponding to the $|1,0\rangle$ eigenvalue is associated with the relaxation time of the S_z component of the electron spin,

$$\lim_{\mathbf{q}\to 0}\frac{1-u^2\Lambda_i}{\tau_0} = \tilde{\tau}_\phi^{-1} + \tau_z^{-1}, \tag{40}$$

where

$$\tau_z^{-1} = 4D_x(\bar{\alpha}^2 + \bar{\beta}^2 + 2\bar{\alpha}\bar{\beta}\sin 2\varphi) + 4D_y(\bar{\alpha}^2 + \bar{\beta}^2 - 2\bar{\alpha}\bar{\beta}\sin 2\varphi). \tag{41}$$

The minimum of this expression as a function of $\bar{\beta}$ is realized for

$$\bar{\beta} = \frac{D_y - D_x}{D_y + D_x}\bar{\alpha}\sin 2\varphi. \tag{42}$$

In particular, when $\bar{\beta} = \bar{\alpha}$, Eq. (42) indicates that propagation with minimum relaxation rate of S_z occurs for angles that satisfy $\sin 2\varphi = 1$ when $D_y > D_x$ and for $\sin 2\varphi = -1$ for $D_x > D_y$. Each one of these cases can be realized by adjusting the miniband width Δ:

$$(\tau_z)_{\rm min}^{-1} = 2(D_x + D_y)\alpha^2\left[1 - \left(\frac{D_x - D_y}{D_x + D_y}\right)^2\sin^2 2\varphi\right]. \tag{43}$$

Two more solutions of the Cooperon equation are obtained from the coupled eigenstates $|11\rangle$ and $|1,-1\rangle$,

$$\lim_{\mathbf{q}\to 0}\frac{1-u^2\Lambda_i}{\tau_0} = \tilde{\tau}_\phi^{-1} + \tau_z^{-1}/2 \pm\sqrt{\left(\tau_z^{-1}/2\right)^2 - 16D_xD_y(\bar{\alpha}^2 - \bar{\beta}^2)^2}, \tag{44}$$

which generate the other two spin-relaxation rates,

$$\tau_\pm^{-1} = \tau_z^{-1}/2 \pm\sqrt{\left(\tau_z^{-1}/2\right)^2 - 16D_xD_y(\bar{\alpha}^2 - \bar{\beta}^2)^2}. \tag{45}$$

When $\bar{\alpha} = \bar{\beta}$, for any value of the angle φ, the four solutions obtained from the Cooperon eigen-equation in the limit $\mathbf{q} \to 0$ become degenerate two by two and the weak localization correction to the conductivity is given only by the terms dependent on τ_z. Furthermore, in the case of the isolated wire, when $D_x = 0$ for the propagation direction that corresponds to $\sin 2\varphi = 0$, $\bar{\beta} = \pm\bar{\alpha}$ and the spin-relaxation rate cancels, a well known result in the physics of SOI systems.[22]

In a LSL system, for significant bandwidth, as seen in Fig. 1, the relationship between $\bar{\beta}$ and $\bar{\alpha}$, expressed in Eq. (42), allows for the minimization of the S_z relaxation rate leading to a regime of *almost free* spin-relaxation transport, similar to what happens in isolated wires. In the special case of $\alpha = \pm\beta$, at angles $\varphi = 3\pi/4$ and $\varphi = \pi/4$, respectively, depending on the relationship between D_x and D_y, the WL correction to the conductivity reduces to that of the system in the absence of SOI.[14]

IV. RESULTS AND DISCUSSION

To illustrate our results, we consider a GaAs LSL with $a = 30$ nm and $n = 2\times 10^{11}$ cm^{-2} as above and use the results of Eqs. (18) in Eqs. (41) and (45) to investigate the variation of the spin-relaxation rates with the miniband width Δ and the orientation angle of the LSL axis φ. Since the two normalized spin-orbit couplings $\bar{\alpha}$ and $\bar{\beta}$ appear in a symmetric fashion, we introduce their ratio $r = \bar{\beta}/\bar{\alpha}$ and plot the normalized scattering rate $1/\tau_{z,\pm}\bar{\alpha}^2$. Their variation with Δ for two values of the angle φ, 0 and $3\pi/4$, are presented in Figs. 2–4. In all cases the evolution of the relaxation rates is strongly affected by the interplay between r and values of the diffusion coefficients D_x and D_y that are determined by Δ. While at $\varphi = 0$, $1/\tau_z\bar{\alpha}$ increases monotonically with r for all values of Δ, as the orientation of the LSL axis is changed

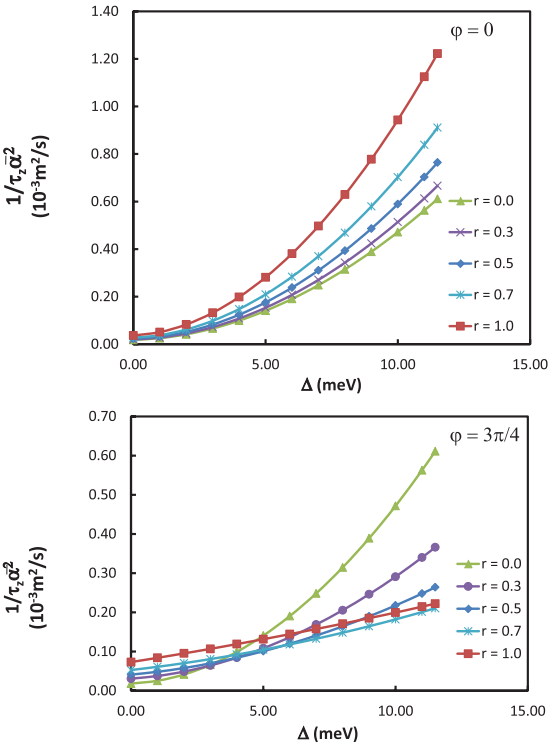

FIG. 2. (Color online) $1/\tau_z\bar{\alpha}$ is plotted as a function of the miniband width Δ (expressed in meV) for different values of $r = \bar{\beta}/\bar{\alpha}$ and orientation angles $\varphi = 0$ and $3\pi/4$.

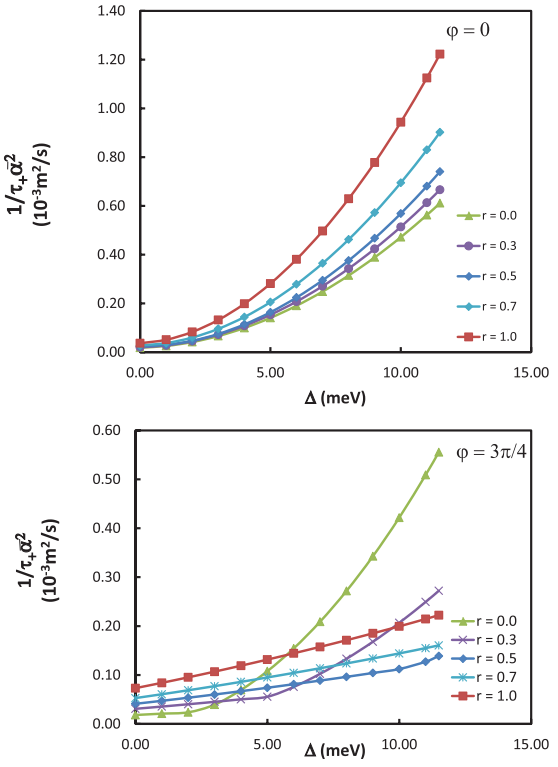

FIG. 3. (Color online) $1/\tau_+\bar{\alpha}$ is plotted as a function of the miniband width Δ (expressed in meV) for different values of $r = \bar{\beta}/\bar{\alpha}$ and two orientation angles $\varphi = 0$ and $3\pi/4$.

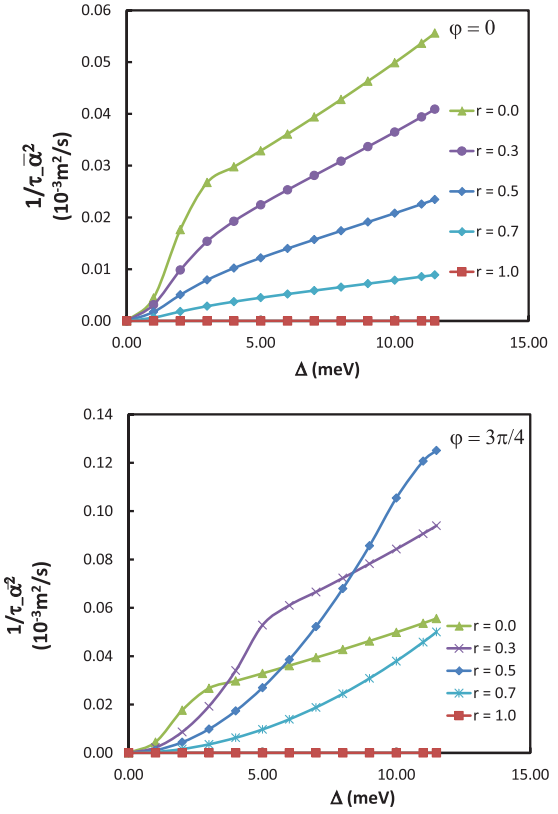

FIG. 4. (Color online) $1/\tau_-\bar{\alpha}$ is plotted as a function of the miniband width Δ (expressed in meV) for different values of $r = \bar{\beta}/\bar{\alpha}$ and orientation angles $\varphi = 0$ and $3\pi/4$.

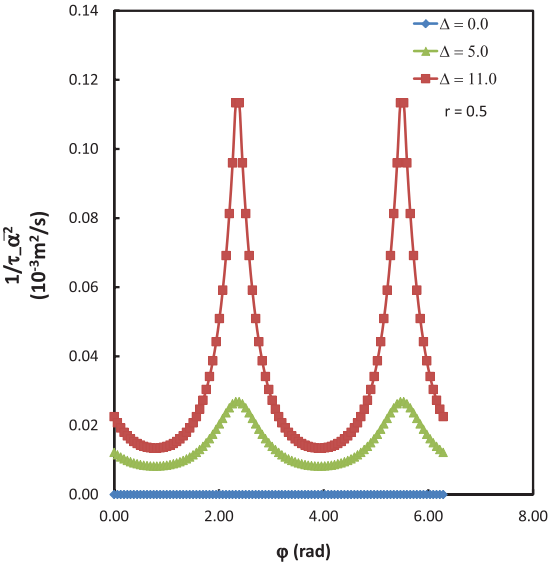

FIG. 5. (Color online) $1/\tau_-\bar{\alpha}$ is plotted as a function of the orientation angle φ for several values of the miniband width Δ (expressed in meV) and $r = \bar{\beta}/\bar{\alpha} = 0.5$.

to $\varphi = 3\pi/4$, as seen in in Fig. 2, its minimum depends both on r and the miniband width, such that for $D_x < D_y$, $r = 0$ generates the lowest value, while at $D_x > D_y$ the lowest value is reached for $r = 0.7$. Similarly, $1/\tau_+\bar{\alpha}$ in Fig. 3 exhibits a monotonic behavior as a function r for the whole range of bandwidths at $\varphi = 0$, while at $\varphi = 3/4$ its lowest values are reached, depending on the value of Δ for several different

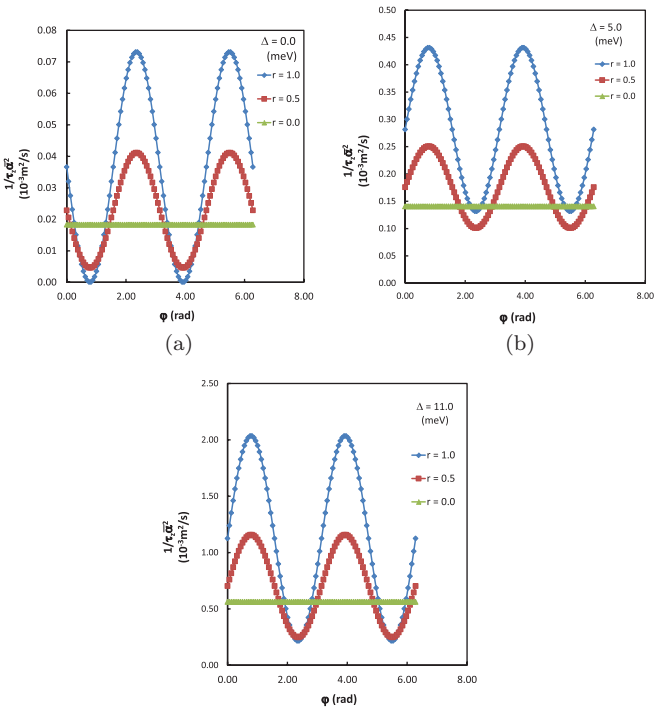

FIG. 6. (Color online) $1/\tau_z\bar{\alpha}$ is plotted as a function of φ for (a) $\Delta = 0.0$ meV, (b) $\Delta = 5$ meV, and (c) $\Delta = 11$ meV.

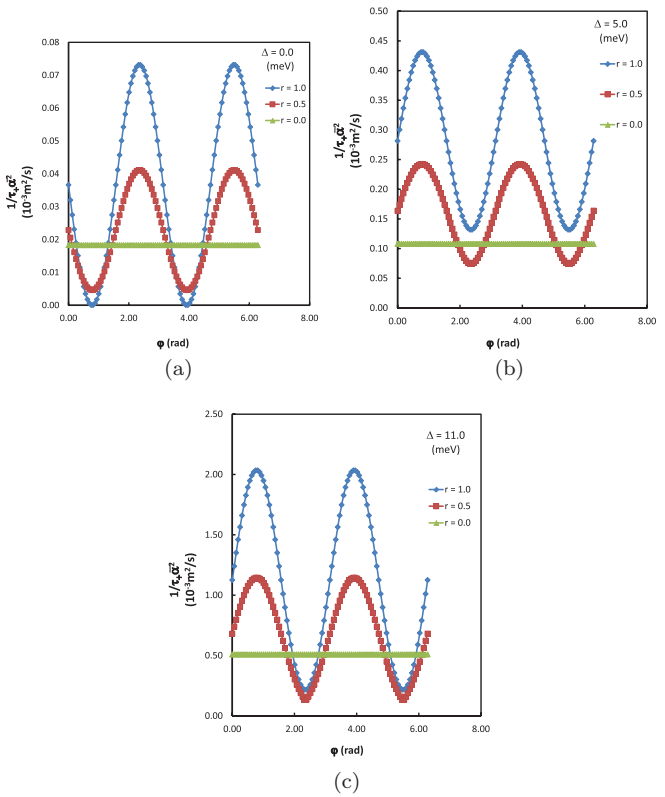

FIG. 7. (Color online) $1/\tau_+\bar{\alpha}$ is plotted as a function of θ for (a) $\Delta = 0.0$ meV, (b) $\Delta = 5.0$ meV, and (c) $\Delta = 11$ meV.

values of r. At the same time $1/\tau_-\bar{\alpha}$ in Fig. 4 decreases with r for all values of Δ at $\varphi = 0$, while at $\varphi = 3\pi/4$ has a nonmonotonic behavior with r, in both cases reaching zero at $r = 1$.

The dependence of the relaxation rates on the orientation angle of the superlattice $\varphi \in [0,2\pi]$ is studied for several values of the miniband width and ratios of the two spin-orbit couplings r. In Fig. 5 we show the variation of $1/\tau_-\bar{\alpha}$ for $r = 0.5$, when it reaches minima for $\varphi = \pi/4$ and $\varphi = 5\pi/4$ for all finite values of the bandwidth. The influence of Δ and r on the minima reached by $1/\tau_z\bar{\alpha}$ can be seen by comparison in Figs. 6(a)–6(c) where shifts in position and amplitude are seen. The same behavior is tracked by $1/\tau_+\bar{\alpha}$ in Fig. 7.

In conclusion, our calculations show that the electron dephasing rate $\tilde{\tau}_\phi^{-1}$ in a lateral superlattice is enhanced compared with the isotropic 2D case by an interference term that originates in the extended Bloch waves along the SL axis. At the same time, the spin-relaxation rates $1/\tau_z$ and $1/\tau_+$ are shown to be degenerate for all values of the miniband width when the strengths of the two SOI couplings are equal. In this situation $1/\tau_- = 0$. The minimum relaxation rates are obtained for finite values of the miniband width for various positions of the LSL axis that depending on the ratio of the two SOI couplings. When $r = 1$ and $D_x \ll D_y$ these findings confirm the experimental results presented in Ref. 10.

ACKNOWLEDGMENT

This work was supported by the Icelandic Research Fund.

[1]C. Albrecht, J. H. Smet, D. Weiss, K. von Klitzing, R. Hennig, M. Langenbuch, M. Suhrke, U. Rössler, V. Umansky, and H. Schweizer, Phys. Rev. Lett. **83**, 2234 (1999).
[2]J. Lobo-Checa, F. Meier, J. H. Dil, T. Okuda, M. Corso, V. N. Petrov, M. Hengsberger, L. Patthey, and J. Osterwalder, Phys. Rev. Lett. **104**, 187602 (2010).
[3]V. Ya. Demikhovskii and D. V. Khomitsky, JETP Lett. **83**, 340 (2006).
[4]P. Földi, V. Szaszkó-Bogár, and F. M. Peeters, Phys. Rev. B **82**, 115302 (2010).
[5]M. Governale and U. Zülicke, Phys. Rev. B **66**, 073311 (2002).
[6]D. V. Khomitsky, Phys. Rev. B **79**, 205401 (2009).
[7]P. Kleinert, V. V. Bryksin, and O. Bleibaum, Phys. Rev. B **72**, 195311 (2005).
[8]D. C. Marinescu and F. Lung, Phys. Rev. B **82**, 205322 (2010).
[9]P. Földi, V. Szaszkó-Bogár, and F. M. Peeters, Phys. Rev. B **83**, 115313 (2011).
[10]S. Z. Denega, T. Last, J. Liu, A. Slachter, P. J. Rizo, P. H. M. van Loosdrecht, B. J. van Wees, D. Reuter, A. D. Wieck, and C. H. van der Wal, Phys. Rev. B **81**, 153302 (2010).
[11]P. Wenk and S. Kettemann, Phys. Rev. B **81**, 125309 (2010).
[12]P. Wenk and S. Kettemann, Phys. Rev. B **83**, 115301 (2011).
[13]F. G. Pikus and G. E. Pikus, Phys. Rev. B **51**, 16928 (1995).
[14]W. Knap, C. Skierbiszewski, A. Zduniak, E. Litwin-Staszewska, D. Bertho, F. Kobbi, J. L. Robert, G. E. Pikus, F. G. Pikus, S. V. Iordanskii, V. Mosser, K. Zekentes, and Y. B. Lyanda-Geller, Phys. Rev. B **53**, 3912 (1996).
[15]B. L. Altshuler, D. Khmel'nitzkii, A. I. Larkin, and P. A. Lee, Phys. Rev. B **22**, 5142 (1980).
[16]S. V. Iordanskii, Y. B. Lyanda Geller, and G. E. Pikus, Pis'ma Zh. Eksp. Teor. Fiz. **60**, 199 (1994).
[17]I. L. Aleiner and V. I. Fal'ko, Phys. Rev. Lett. **87**, 256801 (2001).
[18]D. C. Marinescu, Phys. Rev. Lett. **97**, 176802 (2006).
[19]I. Gradshteyn and I. Ryzhik, *Table of Integrals, Series and Products* (Academic, New York, 2007).
[20]N. W. Aschroft and N. D. Mermin, *Solid State Physics* (Harcourt Brace College, New York, 1976).
[21]M. Suhrke and P. E. Selbmann, Phys. Rev. B **49**, 1908 (1994).
[22]J. Schliemann, J. C. Egues, and D. Loss, Phys. Rev. Lett. **90**, 146801 (2003).